https://doi.org/10.5194/egusphere-2023-1806
Preprint. Discussion started: 19 September 2023

Impacts of synoptic forcing and cloud inhibition on aerosol radiative effect and boundary layer structure during winter pollution in Sichuan Basin, China

Hua Lu[1,3], Min Xie[1,2], Tijian Wang[1], Bojun Liu[4], Yangzhihao Zhan[1], Bingliang Zhuang[1], Shu Li[1], Mengmeng Li[1], Kuanguang Zhu[1,5]

[1]School of Atmospheric Sciences, Nanjing University, Nanjing 210023, China
[2]School of Environment, Nanjing Normal University, Nanjing 210023, China
[3] Chongqing Institute of Meteorological Sciences, Chongqing 401147, China
[4]Chongqing Meteorological Observatory, Chongqing 401147, China
[5]Hubei Provincial Academy of Eco-environmental Sciences, Wuhan 430079, China

Correspondence to: Min Xie (minxie@nju.edu.cn)

Abstract: Winter persistent aerosol pollution frequently occurs in the Sichuan Basin (SCB) due to its unfavorable weather conditions, such as low wind, wetness, and cloudiness. Based on long–term observational data analyses from 2015–2021, it was found that the four representative stations in the SCB often simultaneously experienced $PM_{2.5}$ pollution accompanied by variations in meteorological conditions above 850 hPa, which indicates a connection between regional winter air pollution in the SCB and large–scale synoptic patterns. The dominant 850 hPa synoptic patterns of winter SCB were classified into six patterns using T–model principal component analysis. Pattern 2, characterized by an east high west low (EHWL) pressure system, and Pattern 5, featuring a low trough (LT), were identified as key synoptic patterns for the beginning and accumulation of pollution processes. Pattern 1, characterized by a strong high pressure in the north, was the cleanest pattern associated with reduced $PM_{2.5}$ concentrations. The EHWL and LT patterns were associated with a remarkably high cloud liquid content, which was attributed to upper southerly winds that introduced humid air and converted aerosols into fog/cloud drops. Clouds reduce solar radiation through reflection and scattering, resulting in more stable stratification and aerosol accumulation. This cloud radiation interaction (CRI) is more pronounced in the LT pattern due to denser isobaric lines and stronger southerly winds than in the EHWL pattern. Numerical simulation experiments using WRF-Chem showed afternoon upper–level heating and morning surface cooling forced by the aerosol radiation interaction (ARI) and evening strong surface cooling influenced by valley winds in the SCB. With wet and cloudy synoptic forcing, CRI directly affects the stability of the boundary layer and is

https://doi.org/10.5194/egusphere-2023-1806
Preprint. Discussion started: 19 September 2023

modulated through ARI inhibition. For example, Chongqing showed lower $PM_{2.5}$ concentrations and stronger ARI than the western and southern SCB due to thinner cloud liquid content and weaker CRI inhibition on ARI. The CRI inhibition caused a 50 % reduction in solar radiation and boundary layer height during the daytime under the LT pattern, which was larger than that under the EHWL pattern. This study comprehensively analyzed the cloud inhibition on ARIs and their impacts on the boundary layer structure under typical synoptic forcing during pollution processes, emphasizing the significant role of CRI inhibition in wet and cloudy regions.

Key words: Synoptic patterns, cloud radiation interaction inhibition, aerosol radiation interaction, boundary layer structure, Sichuan Basin.

1 Introduction

Particulate matter (PM) pollution has become a significant environmental concern in China (Xie et al., 2016a; 2016b; Che et al., 2019). High concentrations of aerosols worsen air quality and seriously harm resident health, and affect weather and climate through their effects on radiation and clouds (Li et al., 2019; Zhao et al., 2020; Alexeeff et al., 2021; Yang et al., 2021). The interactions between aerosols and clouds present the largest uncertainty in anthropogenic radiative forcing of the Earth's climate (Liao et al., 2017; Haywood et al., 2021). Understanding cloud aerosol radiation interactions (ARI) from an air quality perspective is crucial for a scientific understanding of the relationship between weather and pollution.

Although excessive emissions are the primary cause of air pollution, local emissions do not commonly change significantly in a short time. However, pollutant concentrations often vary considerably, indicating that meteorological conditions largely govern the pollutant distribution (Zhu et al., 2018; Luo et al., 2018; Nichol et al., 2020; Zhang et al., 2020; Jiang et al., 2021). PM and gaseous pollutants, carried mainly by the planetary boundary layer (PBL), are directly or indirectly influenced by meteorological factors such as wind, relative humidity, PBL height, and solar radiation. These factors contribute to the multi–temporal and spatial distribution characteristics through vertical and horizontal diffusion, physicochemical reactions, and dry and wet deposition (Park et al., 2017; Shu et al., 2017; Zhan et al., 2019; Huang et al., 2019). Large–scale synoptic forcing is considered the primary driving condition for meteorological

https://doi.org/10.5194/egusphere-2023-1806
Preprint. Discussion started: 19 September 2023

factors, PBL structure, and the resulting distribution of atmospheric pollutants (Miao et al., 2019; Ning et al., 2019; Jiang et al., 2020; Li et al., 2021). Specific synoptic patterns can induce advection, which largely determines the local PBL structure and development. PBL, located at the bottom of the atmosphere, is responsible for the main exchange of heat, moisture, and matter between the surface and the free troposphere (Stull, 1988). The fate of pollutants emitted near the surface, a significant source of aerosols in the air, is largely controlled by the PBL (Garratt, 1994). The PBL height is often used to characterize the capacity and dilution of pollutants (Seidel et al., 2010). Synoptic patterns can directly determine the meteorological conditions of emitted pollutants and influence their transport by regulating PBL thermal stratification and mechanical turbulence (Stull, 1988; Ning et al., 2018; Zhan et al., 2019; Jiang et al., 2021; Zhang et al., 2022).

Unfavorable meteorological conditions contribute to aerosol pollution. When pollutants accumulate to a certain degree, aerosols reduce surface solar radiation by backscattering or absorbing solar radiation, leading to surface cooling. This decrease in solar radiation and temperature near the ground weakens turbulent diffusion, suppresses the convective development of the PBL, and lowers PBL height, which in turn exacerbates aerosol pollution (Ding et al., 2016; Wang et al., 2018). Moreover, the increase in humidity caused by the decreased surface saturation vapor pressure and inhibited water vapor diffusion enhances aerosol hygroscopic growth accelerates liquid–phase and heterogeneous reactions, and contributes to aerosol pollution (Pilinis et al., 1989; Zhong et al., 2018; Zhong et al., 2019). This positive feedback between unfavorable PBL meteorology and increasing aerosols explained the majority of the increase in $PM_{2.5}$ during cumulative stages (Zhong et al., 2018). As for the aerosol-cloud interactions, arise from increasing aerosols acting as cloud condensation nuclei in cloud and translating into larger concentrations of smaller cloud droplets, leading to an increased cloud albedo reflecting more radiation back to space(Twomey, 1977; Lohmann and Feichter, 2005). Even a marginal increase in cloud droplets above pristine conditions in deep convective clouds causes more droplets to reach supercooled levels, which enhances latent heat release and invigorates convection (Rosenfeld et al., 2009; Possner et al., 2015). Further increases in cloud droplets result in direct radiative effects, reducing downward solar radiation, cooling the surface, and inhibiting convection (Scott et al., 2016).

https://doi.org/10.5194/egusphere-2023-1806
Preprint. Discussion started: 19 September 2023

The Sichuan Basin (SCB) is surrounded by high mountains with cloudy and wet weather conditions. The mean annual relative humidity, cloud cover, and sunshine hours for the SCB are 75 %, 8 h, and 1200 h, respectively. The Chengdu–Chongqing city cluster in the SCB serves as the economic center of the upper reaches of the Yangtze River in China, accounting for approximately 10 % of the population of the country. Rapid industrialization and urbanization in this region have resulted in severe air pollution, making it one of the most polluted regions in China with high black carbon concentrations (Li et al., 2016; Cao et al., 2021). The Qinghai–Tibet Plateau on the western edge of the SCB significantly influences the transport and accumulation of pollutants through thermal and dynamic effects (Ning et al., 2017; Shu et al., 2021). In addition, the Qinghai–Tibet topography leads to higher cloud water content over the SCB than the other regions (Yu et al., 2004; Yang et al., 2012). Complex terrain and higher cloud water content may modify aerosol–PBL interactions, alter cloud chemistry, and affect the distributions of pollutants and $PM_{2.5}$ chemical components, thus impacting ARIs (Zhao et al., 2017; Wang et al., 2018). The positive effects of aerosols and PBL meteorology can be influenced by synoptic patterns (Miao et al., 2020) and inhibited by cloud direct radiative effects in the SCB (Zhong et al., 2019).

Therefore, with high aerosol loadings and semi–permanent cloudy weather, the SCB provides an optimal region for studying the influence of synoptic forcing on the interactions between clouds, aerosols, and the PBL. This study objectively classifies the synoptic patterns influencing the SCB based on long–term data. An integrated analysis of pollutants and meteorological factors reveals the primary pollution sources and clean synoptic patterns. Using WRF–CHEM simulation experiments, the impacts of synoptic forcing and inhibition of cloud radiation interaction (CRI) on ARI with the PBL in the SCB are discussed. These results will deepen our understanding of CRI, ARI, and the PBL interactions in regions influenced by plateau–basin topography with wet and cloudy weather. The data and methods are presented in Section 2, whereas Section 3 describes the synoptic patterns and their corresponding impacts on clouds, aerosols, radiation, and PBL. Finally, the conclusions are presented in Section 5.

https://doi.org/10.5194/egusphere-2023-1806
Preprint. Discussion started: 19 September 2023

2 Data and method

2.1 Observation data

Air quality monitoring data were obtained from air quality monitoring sites established by the Ministry of Ecology and Environment of China across the SCB. Hourly $PM_{2.5}$ observations from 18 stations in the SCB were collected during the winter period from 2015–2021 for data analysis and model verification (Fig. 1b). CQ, CD, MY, DY, LS, MS, YA, ZY, ZG, YB, LZ, NJ, GA, NC, SN, GY, DZ, and BZ represent Chongqing, Chengdu, Mianyang, Deyang, Leshan, Meishan, Yaan, Ziyang, Zigong, Yibin, Luzhou, Neijiang, Guangan, Nanchong, Suining, Guangyuan, Dazhou, and Bazhong, respectively.

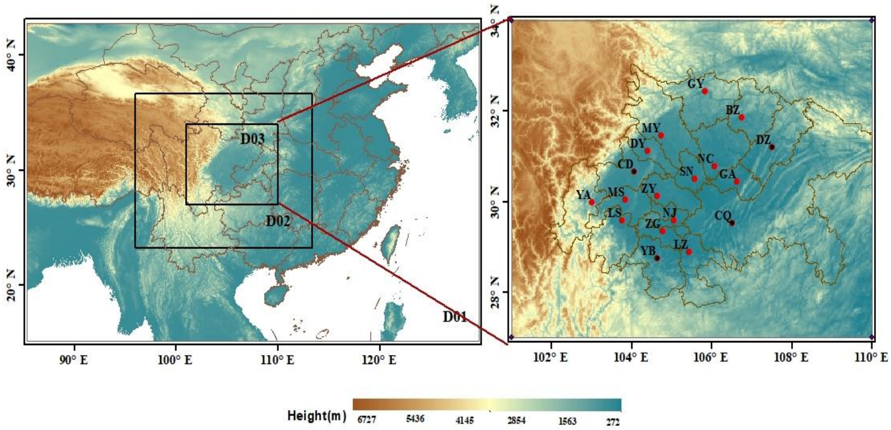

Figure 1. (a) Three layers of simulation domains in WRF-Chem with topography map as shading; (b) the locations of 18 air quality monitoring stations(red dots) and 4 sounding stations(black dots) in the Domain 3.

The SCB has four sounding stations: Wenjiang (Chengdu), Yibin, Dazhou, and Shapingba (Chongqing), situated in the western, southern, northwestern, and eastern regions of the basin, respectively (Fig. 1b), representing different pollution and meteorological conditions within the SCB. The vertical distribution of the meteorological factors used in the study was obtained from an L–band sounding radar, collecting temperature, pressure, humidity, and wind data at 0800 and 1200 local time on vertical levels every second from the surface up to 30 km. Ground observation data from the four cities, including temperature and dew point temperature, were used for

https://doi.org/10.5194/egusphere-2023-1806
Preprint. Discussion started: 19 September 2023

meteorological factor simulation verification. All meteorological data were obtained from the China Weather Website Platform maintained by the China Meteorological Bureau.

ERA5 reanalysis data from the ECMWF, which assimilates comprehensive observation data, including ground observation, sounding data, aircraft observation data, and satellite observation data, were obtained for synoptic pattern classification and their impact on meteorological factors in four representative cities. The EAR5 data at the 850 hPa pressure level were collected for the synoptic pattern study. Additionally, cloud liquid water content, downward solar radiation, and boundary layer height derived from the EAR5 single–level datasets were obtained to assess the influences of synoptic forcing on CRI studies, while PBL height were adopted to conduct the simulation verification.

2.2 Synoptic pattern classification

The objective classification was conducted on the synoptic patterns of the SCB using ERA5 data, including geopotential height, u, and v components of winds at the 850 hPa pressure level. The analysis covered an area of 97–117° E and 24–37° N with a horizontal resolution of 0.25° × 0.25°. Since PM pollution in the SCB primarily occurs in winter (Zhao et al., 2018; Lu et al., 2022b), the synoptic pattern classification was performed for winter 2015–2021 (December, January, and February) using the principal component analysis in the T–model (T–PCA) objective method. Compared with the subjective classification method, the objective method can process large amounts of data without relying on subjective experience (Huth et al., 2008; Miao et al., 2017). Among various classification methods, the T–PCA method accurately reflects the characteristics of the original synoptic circulations and exhibits spatial and temporal stability (Huth et al., 1996; Huth et al., 2008). Consequently, the T–PCA has been widely used in synoptic pattern classification research (Ning et al., 2019; Miao et al., 2020; Li et al., 2021).

2.3 Model configuration and simulation experiments

To understand the combined effects of synoptic patterns and CRI inhibition on ARI and PBL, a series of parallel experiments were conducted on the simulation of a typical pollution episode using the Weather Research and Forecasting model with Chemistry (WRF–Chem v3.9.1) (Grell et al., 2005). The model domain (Fig. 1a) was centered over the SCB and utilized three layers of

https://doi.org/10.5194/egusphere-2023-1806
Preprint. Discussion started: 19 September 2023

nested grids with cell points of 155×110 (D01), 184×160 (D02), and 320×250 (D03). The horizontal resolutions of the model were 27, 9, and 3 km for the three layers, while 32 vertical layers spanning from the surface to 100 hPa were defined. Initial meteorological fields were obtained from the National Centers for Environmental Prediction Final reanalysis data with a horizontal resolution of 1° × 1° and 6 h time interval. For chemical process simulations, anthropogenic emissions were sourced from the Multiresolution Emission Inventory for China (MEIC) in 2016, featuring a grid resolution of 0.25° × 0.25°. Biogenic emissions were calculated online using the Guenther scheme (Guenther et al., 2006). Table 1 provides a summary of the chosen physical and chemical parameterization schemes.

Table 1 The main options of WRF–Chem

Items	**Contents**
Microphysics	WRF Single–Moment 5 class (WSM5) scheme
Longwave radiation	RRTMG scheme (Iacono et al., 2008)
Shortwave radiation	RRTMG scheme (Iacono et al., 2008)
Planetary boundary layer	Younsei University scheme (Hong et al., 2006)
Land surface	United Noah land surface model (Tewari et al., 2004)
Cumulus parameterization	Grell–Freitas ensemble scheme (Grell et al., 2013)
Gas–phase chemistry	RADM2 (Stockwell et al., 1990)
Aerosol module	MADE/SORGAM (Schell et al., 2001)

To assess the impact of CRI inhibition on ARI and ARI under typical synoptic pollution patterns, four parallel experiments were conducted to simulate the pollution process. The selected simulation period is January 1-7, 2017, as the period is close to the time of MEIC emission inventory used. Besides, the Chinese government announced clean air action in 2013 with the goal of reducing $PM_{2.5}$ pollution in key areas by controlling anthropogenic emission sources within a five-year period, with the year of 2017 as the key year about current $PM_{2.5}$ pollution (Wang et al., 2020). Finally, the period of January 1-7, 2017 encompasses both typical pollution and clean weather patterns. Considering these three factors, this study focuses on

https://doi.org/10.5194/egusphere-2023-1806
Preprint. Discussion started: 19 September 2023

simulation and analysis during this period. The baseline experiment (BASE) considered both CRI and ARI, while the three sensitivity experiments excluded ARI or CRI. Experiment 1 (EXP1) did not include ARI, Experiment 2 (EXP2) did not consider CRI, and Experiment 3 (EXP3) did not consider ARI when CRI was not excluded. The differences between BASE and EXP1 represented the disturbances caused by ARI, while EXP2 and EXP3 represented the influences of ARI without CRI inhibition. The numerical experiments ran from 00:00 UTC on December 30, 2016, to 00:00 UTC on January 8, 2017, with the initial 48 h used for a model spin–up.

3 Results and discussions

3.1 Relationships between synoptic patterns and $PM_{2.5}$ pollution in the SCB

Figure 2 illustrates the daily mean variations in $PM_{2.5}$ concentration and vertical distributions of potential temperature (PT) during winter from 2015 to 2021, highlighting the pollution episodes. The four sounding stations in the SCB (CD, YB, CQ, and DZ) are located in separate areas of the basin; however, they consistently experienced pollution processes with simultaneous changes in vertical thermal structures. For example, during the pollution events in January 2017 and December 2020, $PM_{2.5}$ concentrations in all four cities reached their highest levels at the same time before declining rapidly (Fig. 2). Notably, the warming of the upper air coincided with pollution episodes, while a decrease in $PM_{2.5}$ concentration correlated with cooling in the upper layer. Despite the significant distances between these cities (approximately 200–400 km), the synchronized changes in pollutants and vertical thermal structures can be attributed to large–scale synoptic patterns (Miao et al., 2020; Li et al., 2021). While the four cities with sounding stations were selected as representatives for vertical thermal structure analysis, other cities in the SCB also experienced pollution episodes and relevant physical processes.

https://doi.org/10.5194/egusphere-2023-1806
Preprint. Discussion started: 19 September 2023

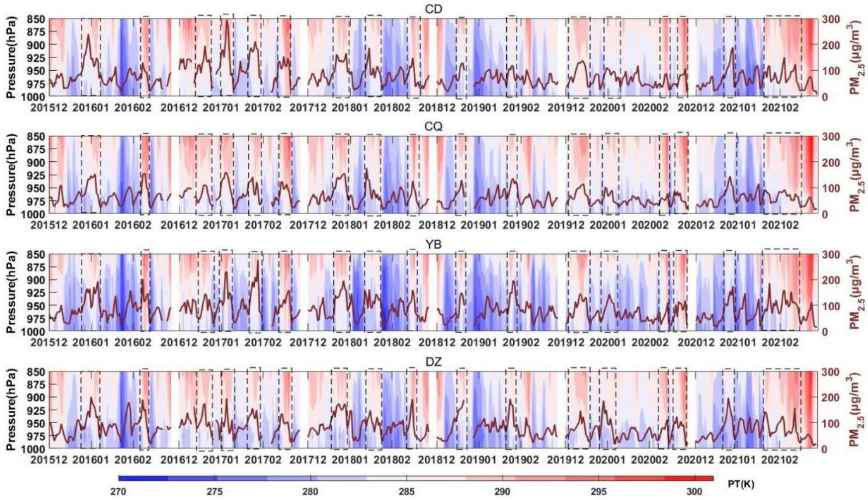

Figure 2. Time series of $PM_{2.5}$ and potential temperature derived from the sounding data during 2015-2021 winter months. The $PM_{2.5}$ pollution episodes are marked with black dotted boxes.

The time series of $PM_{2.5}$ from air quality monitoring sites and the accompanying vertical distributions of temperature, relative humidity, and wind in CD, CQ, YB, and DZ derived from the sounding stations are shown in Fig. 3, using January 2017 as an example for analysis. During this month, two severe $PM_{2.5}$ pollution episodes occurred: January 1–7 and January 24–31 in 2017. The highest daily $PM_{2.5}$ concentrations recorded were 291.17 μg/m^3 (CD) and 276.21 μg/m^3 (YB), influencing all four cities. Pollution in early January exhibited a gradual increase in $PM_{2.5}$ levels from January 1–3, with upper air warming and the emergence of an inversion above the PBL. Additionally, lower humidity and higher wind speeds above 1500 m were observed during the pollution accumulation period. Similarly, the late January pollution episode showed a rapid increase in $PM_{2.5}$, from January 24–27, together with warming, dryness, and high wind speed above 1500 m in all four cities. These consistent meteorological conditions during the pollution periods indicate significant synoptic forcing. Notably, the key layer for studying the connection between synoptic patterns and $PM_{2.5}$ pollution is approximately 850 hPa, corresponding to a height of approximately 1500 m within the PBL, where changes in specific meteorological conditions primarily affect surface–emitted pollutants.

https://doi.org/10.5194/egusphere-2023-1806
Preprint. Discussion started: 19 September 2023

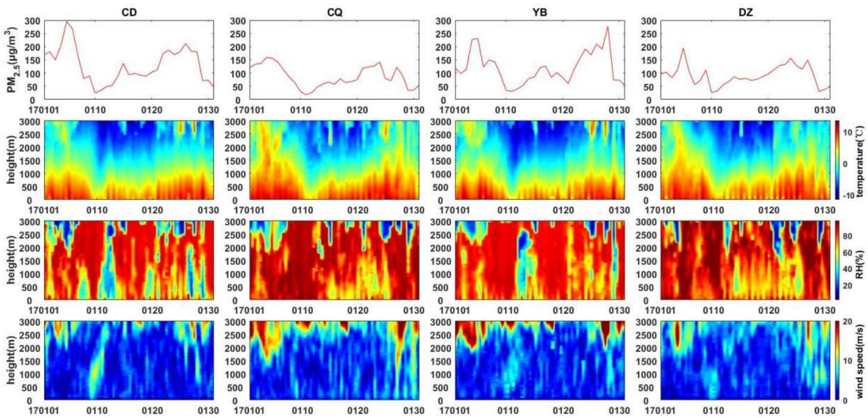

Figure 3. Time series of (a)$PM_{2.5}$ concentrations, and corresponding vertical meteorological data from the sounding data, including (b)vertical temperature, (c)vertical humidity and (d)vertical wind speed, taking January 2017 as an example to illustration.

Using ERA5 reanalysis data for winter (December, January, and February) from 2015 to 2021, the 850 hPa synoptic patterns over the SCB were objectively classified into six types (Fig. 4). According to the relative positions of the high–pressure and low–pressure systems in the basin, these synoptic patterns can be described as follows: (1) strong high pressure in the north, (2) east high west low (EHWL) pressure, (3) weak high pressure in the north, (4) weak ridge of high pressure after the trough, (5) low trough (LT), and (6) strong high pressure. Patterns 1 and 3 exhibit high pressure in the northern SCB, which differs from the high–pressure intensity. With strong high pressure, the basin is primarily controlled by northerly airflow. Under weak high–pressure conditions, the basin is dominated by an easterly backflow. Patterns 2 and 5 had high and low pressures near the basin, forming a relatively dense isopotential altitude gradient and resulting in strong southerly winds over 850 hPa. Pattern 4 was a weak high–pressure ridge after a trough controlled the SCB with sparse isobaric lines and weak winds leading to static and stable weather conditions. During Pattern 6, the SCB was controlled by the cold high-pressure system, accompanying weak northerly airflow on the basin. Pattern 6 usually evolved from either Pattern 1 or Pattern 3.

https://doi.org/10.5194/egusphere-2023-1806
Preprint. Discussion started: 19 September 2023

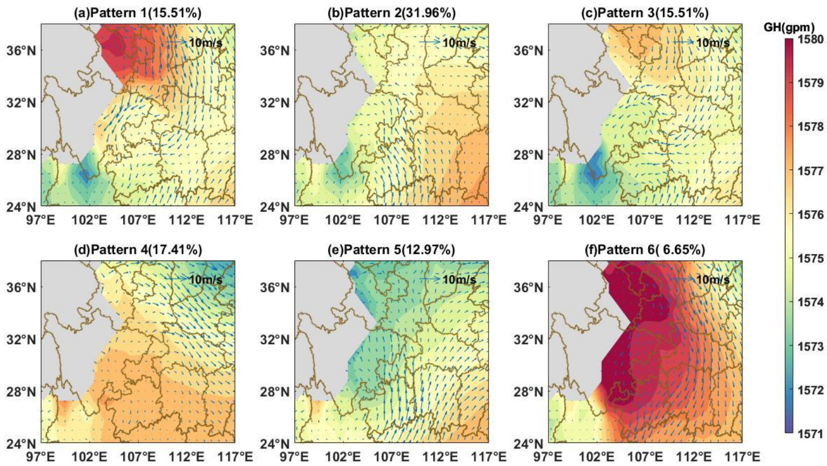

Figure 4. The 850hPa geopotential height field(shading) with wind vector fields(blue vectors), and frequency of occurrence for 6 synoptic patterns during 2015-2021 winter months.

Patterns 2, 4, and 5 exhibited higher frequencies of pollution occurrence ($PM_{2.5}$ daily concentration ≥ 75 μg/m^3) according to statistical results from 18 cities in the SCB during the 2015–2021 winters (Fig. 5a). These patterns were associated with high $PM_{2.5}$ concentrations in 50–70 % days, including CD, DY, and MY in the northern SCB, 40–60 % for cities in the southern SCB, such as ZG and YB, and also 40–60 % of days for cities in the northern SCB, such as CQ, DZ, NC, and GA. Furthermore, the average $PM_{2.5}$ concentrations in the respective cities for the six synaptic patterns were calculated (Fig. 5b), aligning with the frequency of pollution occurrence. The days under Patterns 2, 4, and 5 exhibited higher average daily $PM_{2.5}$ concentrations. The average concentrations of CD, YB, CQ, and DZ under these three synoptic patterns were 99.19, 103.43, and 111.97 μg/m^3, 95.44, 87.98, and 94.26 μg/m^3, 79.14, 83.96, and 74.771 μg/m^3, and 91.02, 104.64, and 91.51 μg/m^3, respectively. Regarding the impact of synoptic patterns on the accumulation or dispersion of $PM_{2.5}$, Fig. 5c illustrates the average daily changes in $PM_{2.5}$ concentration compared with the previous day for CD, CQ, YB, and DZ under the six synoptic patterns. Patterns 2 and 5 exhibited the most significant $PM_{2.5}$ accumulation under the influence of southerly airflow.

https://doi.org/10.5194/egusphere-2023-1806
Preprint. Discussion started: 19 September 2023

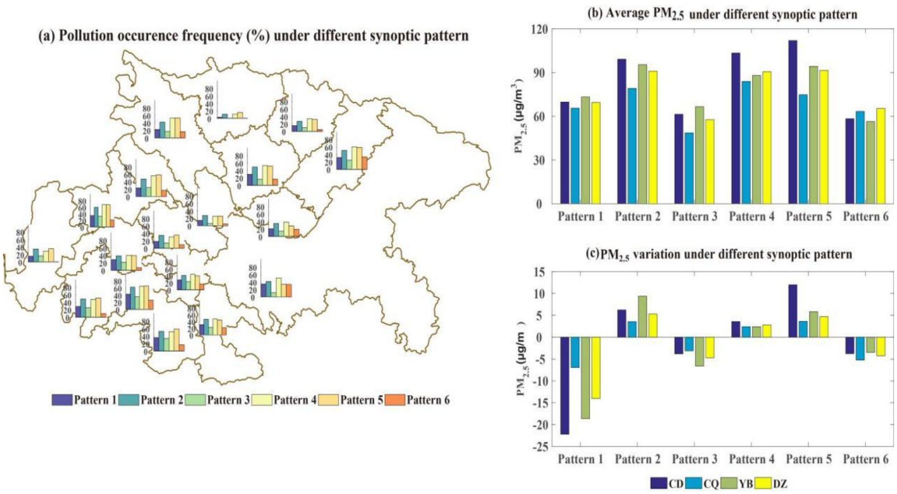

Figure 5. (a)The pollution occurrence frequency at 18 air pollution stations in SCB, (b)(c)average $PM_{2.5}$ concentrations and $PM_{2.5}$ day to day variations at 4 representative SCB cities, under 6 synoptic patterns.

The time series of $PM_{2.5}$ and the day-to-day classification of 850 hPa synoptic patterns are shown in Fig. 6, from December 2016 to January 2017. Six pollution episodes occurred during this period (December 03–12 and 16–26, 2016; January 1–7, 16–19, and 20–28, 2017; and February 14–23). It is evident that pollution episodes consistently began with Pattern 2 and ended with Pattern 1, accompanied by a rapid decline in $PM_{2.5}$, suggesting that Pattern 2 is the key synoptic forcing for pollution initiation. Statistical results revealed that Pattern 2 accounted for a high proportion of $PM_{2.5}$ increase in the six pollution episodes, reaching 48.48 %, while Pattern 5 had the second highest proportion of 21.88 %, with Patterns 2 and 5 combined accounting for more than 70 %. For example, during the two heavy pollution events that occurred in early and late January 2017, $PM_{2.5}$ rapidly accumulated with the interplay of Patterns 2 and 5. In addition, Patterns 2 and 5 represented a significant proportion of 31.96 % and 12.97 %, respectively (Fig. 4), during winters from 2015 to 2020 over 850 hPa in the SCB. Based on this analysis, Patterns 2, 4, and 5 were identified as synoptic pollution patterns, whereas Patterns 1, 3, and 6 were clean. Patterns 2 and 5 played crucial roles in the initiation and accumulation of $PM_{2.5}$ during pollution episodes.

The disscusion above showed that pollution in the SCB usually occurred when airflow controlled the upper-layer of the basin (Pattern 2 and 5), while the dispersion of pollutants was

https://doi.org/10.5194/egusphere-2023-1806
Preprint. Discussion started: 19 September 2023

accompanied by northerly winds, which is consistent with Lu et al. (2022a). Southerly airflow in the upper-layer could bring warm air, leading to warming above the basin and forming a warm lid. Combined with the surrounding mountains and plateau, a relative enclosed space could be formed in the SCB, resulting in local circulations and allowing for the thorough mixing and secondary reactions of local emission and pollutants transported from outside. As a result, persistent and severe pollution often occurred under the influence of southerly airflow. When the northerly airflow begin to dominate the SCB, the warm lid and local circulation were disrupted, leading to dispersion of pollutants through advection and vertical transport. Additionally, northerly winds are often associated with cold air and sometimes accompanied by weak precipitation, resulting to wet deposition. Therefore, the arrival of northerly airflow often signifies the ending of the pollution episode.

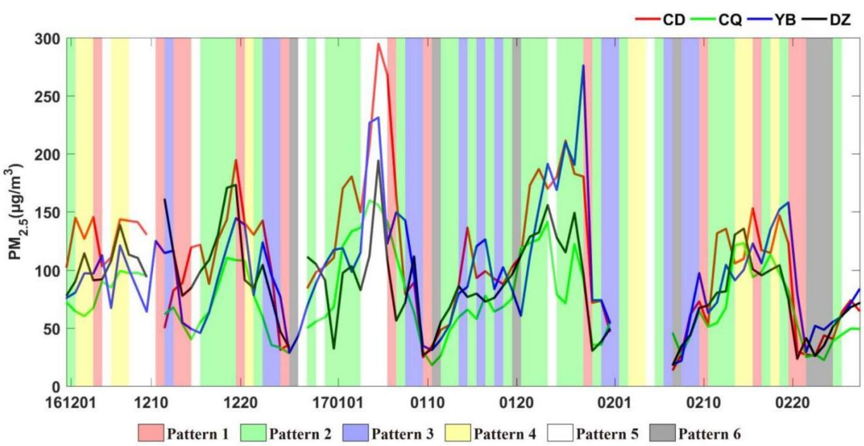

Figure 6. Time series of $PM_{2.5}$ concentrations and the day to day 850hPa synoptic patterns at 4 representative SCB cities, taking December 2016 to February 2017 as an example for illustration.

Because of the convergence of air moving eastward across the Tibetan Plateau, the SCB experiences a high frequency of wet and cloudy weather, with cloud cover fraction exceeding 80 % (Yu et al., 2004; Zhang and Lin, 1985). The roles of clouds in the interactions of aerosols, radiation, and the PBL under typical synoptic forcing must be non–negligible in this region. This study evaluated the average cloud liquid water content, downward solar radiation, and PBL under the influence of the six classified synoptic patterns in CD, CQ, DZ, and YB, using data from

https://doi.org/10.5194/egusphere-2023-1806
Preprint. Discussion started: 19 September 2023

ERA5 (Fig. 7). Reanalysis data revealed significantly higher cloud liquid water contents with Patterns 2 and 5, likely triggered by robust southerly air prevailing at 850 hPa over the SCB (Fig. 4). This southerly air brings warm and moist air, contributing to cloud formation. Dense clouds reduce solar radiation through reflection and scattering, resulting in surface cooling and inhibiting PBL development. The PBL height under Patterns 2 and 5 was approximately 900–1000 m, lower than that under the influence of clean synoptic Pattern 1 at 1500 m (Fig. 7). In contrast, the clean synoptic Pattern 1 is characterized by a strong northerly flow at 850 hPa, resulting in lower cloud liquid water content over the basin and increased solar radiation, promoting PBL development. The lower PBL height with more stable stratification caused by the CRI in Patterns 2 and 5 can partially explain the rapid accumulation of $PM_{2.5}$ during these two pollution patterns.

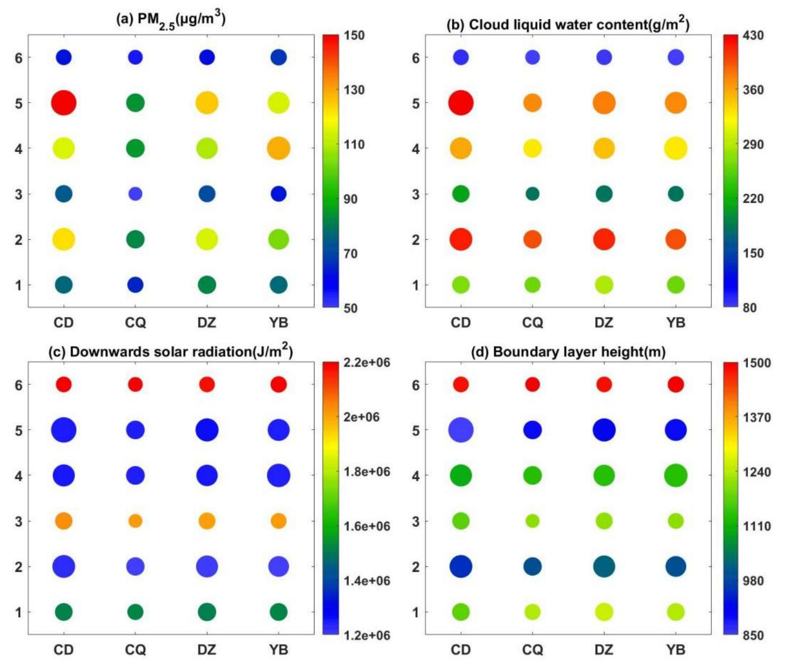

Figure 7. The averaged (a)$PM_{2.5}$ concentrations, (b)cloud liquid water contents, (c)downwards solar radiation and (d)boundary layer height derived from 2015-2021 winter months ERA5 reanalysis data, at 4 representative SCB cities under 6 synoptic patterns, the dot sizes represent $PM_{2.5}$ concentrations.

https://doi.org/10.5194/egusphere-2023-1806
Preprint. Discussion started: 19 September 2023

3.2 Integrate impacts of synoptic patterns and the CRI inhibition on ARI

Based on the above analysis, Patterns 2 and 5 were identified as the key pollution synoptic patterns accompanying dense clouds and, thus, CRI. However, the effects of pollution patterns on ARI and their interaction with CRI in the SCB remain unclear and warrant further investigation. A typical pollution episode from January 1–7, 2017, was selected to understand these complex processes and simulated using WRF–Chem. The BASE simulations were verified with observations to determine the accuracy and reliability of the simulation results. The simulated $PM_{2.5}$, T2, and TD2 values at the four representative stations from January 1–7 are shown in Fig. 8. The evaluation demonstrated that the simulation captured changes in relevant elements in the SCB, representing variations in $PM_{2.5}$ and meteorological conditions. In addition, the vertical profiles of potential temperature and relative humidity in the model were compared with the sounding data from the SCB (Fig. 9). The simulation aligned well with the sounding observations, reflecting upper air warming and PBL humidification during the accumulation process of $PM_{2.5}$, as well as upper air cooling with PBL drying during the dissipation process of $PM_{2.5}$. Differences between simulation and observation in surface wind could be predictable in case of low wind and complex terrain. In addition, this could also be attributed to the negligence of WRF model in considering the atmospheric drag to that generated by vegetation produced by the unresolved topographic features (Zhan et al., 2023). As for the vertical wind profile, simulation results could capture the shift in winds and reproduce the height-time patterns in whole despite some differences. For the verification of PBL height, sounding data are commonly regarded as reliable vertical observation and PBL height can be calculated based on sounding data, however the low temporal resolution of sounding data made it not suitable to be adopted to compared with refined variations of PBL height in this study. Besides, PBL height derived from ERA5 shows good consistency with sounding data in the SCB based on long-term validation(Guo et al., 2016). As a result, PBL height derived from the ERA5 has been added in Figure 9(a)-(d) to verify the simulations in Figure 9(e)-(h). The certain values of PBL height simulations differed from ERA5 data, but the magnitudes and change trends aligned well. Overally, although discrepancies existed, the simulation generally reproduced the observations of both pollutants and meteorological factors during this pollution episode, providing a reliable basis for subsequent analysis.

https://doi.org/10.5194/egusphere-2023-1806
Preprint. Discussion started: 19 September 2023

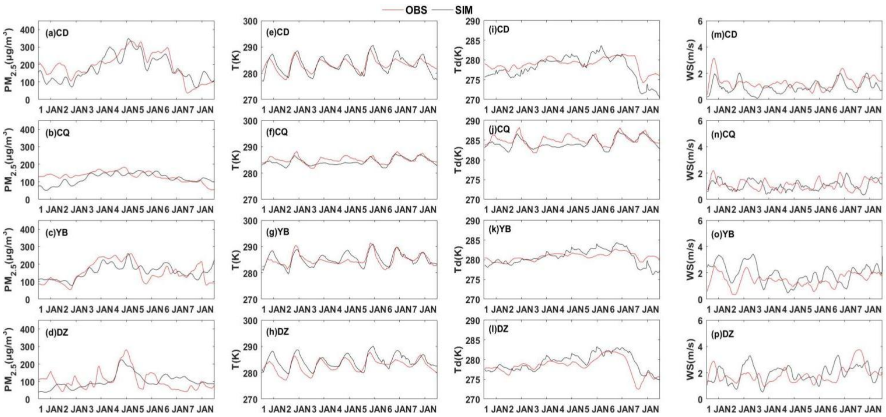

Figure 8. Time series of simulated and observed (a)-(d)$PM_{2.5}$ concentration, (e)-(h)temperature at 2m, (i)-(l) dew temperature at 2m and (m)-(p)wind speed at 4 representative SCB cities during 1-7 January 2017.

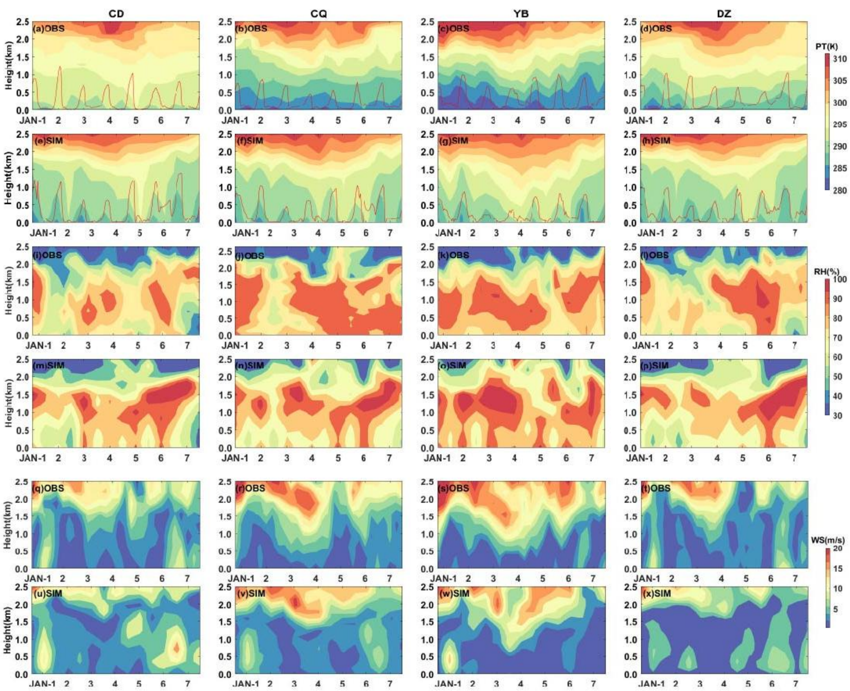

Figure 9. Simulated and observed time-height sections of (a)-(h) potential temperature, (i)-(p)relative humidity and (q)-(x)wind speed at 4 representative SCB cities during 1-7 January 2017. The red lines in (e)-(h) are time series the boundary layer heights derived from simulation.

https://doi.org/10.5194/egusphere-2023-1806
Preprint. Discussion started: 19 September 2023

During the pollution episode from January 1–7, 2017, the pollution synoptic pattern controlled the SCB on January 1–6, with Pattern 2 on January 1–3, Pattern 5 on January 4–6, and Pattern 1 on January 7 (Fig. 6). Consequently, $PM_{2.5}$ pollution in the SCB occurred on January 1–6 and rapidly dissipated on January 7 (Fig. 8). The mean geopotential height at 850 hPa derived from the simulation of January 1–3 under Pattern 2 showed EHWL, with southerly flow prevailing over the SCB (Fig. 10a). The resulting upper air warming suppressed PBL development (Fig. 9). During January 1–3 under Pattern 2, the average PBL heights were lower (Fig. 11a), acting as a lid above the SCB and hindering the airflow within the basin due to the surrounding mountains. Low wind speeds provided adverse diffusion conditions for pollutants emitted into the basin, resulting in severe pollution in the western and southern SCB (Fig. 11d). As for January 4–6, the low pressure over the SCB evolved into an LT pattern, termed Pattern 5 in the previous analysis. Compared with Pattern 2, the isobaric lines were denser under the influence of the LT, leading to stronger southerly winds above the SCB (Fig. 10a–b). Lower average PBL heights appeared during January 4–6 under Pattern 5 compared with those of January 1–3 under Pattern 2 (Fig 11a–b), which is attributed to stronger upper air warming and more stable stratification (Fig. 9a–h). The pollutants accumulated during January 4–6 from the pollution episode that began on January 1–3 (Fig. 11d–e). On January 7, high pressure in the north dominated the SCB with a prevailing northerly flow over the basin (Fig. 10c). The PBL height quickly increased due to upper layer cold advection (Fig. 11c), resulting in a rapid decrease in $PM_{2.5}$ (Fig. 11f). Overall, synoptic patterns played a key role in the accumulation and diffusion of $PM_{2.5}$ during pollution episodes by modulating PBL development and stratification stability.

https://doi.org/10.5194/egusphere-2023-1806
Preprint. Discussion started: 19 September 2023

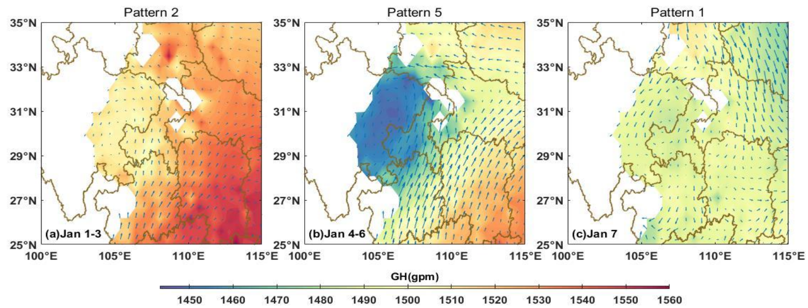

Figure 10. The 850hPa geopotential height field(shading) with wind vector fields(blue vectors) on (a)1-3 , (b)4-6 and (c)7 January, representing 3 typical synoptic patterns in the SCB respectively.

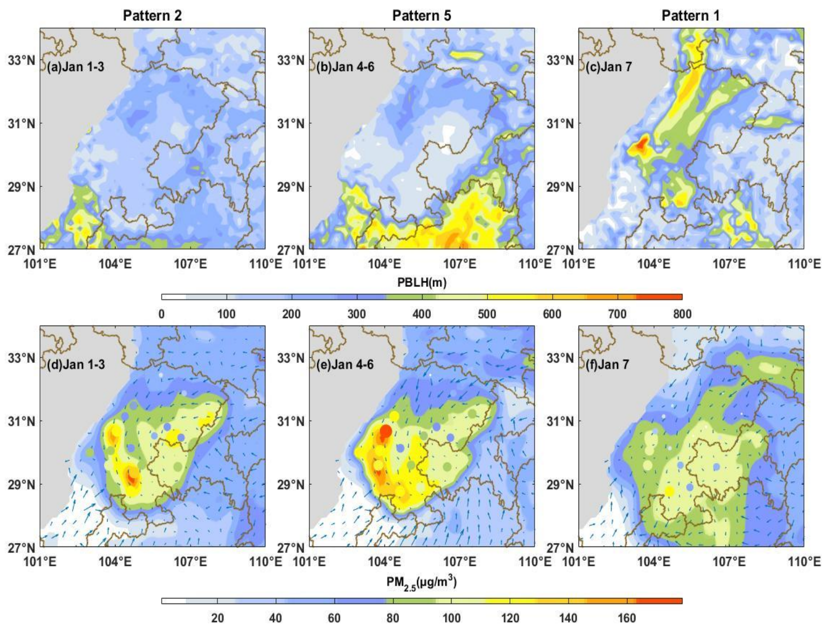

Figure 11. The simulated (a)-(c)boundary layer height and (d)-(f)$PM_{2.5}$ concentrations(shading) and wind vector fields at 900hPa(blue vectors) for 1-3, 4-6 and 7January. The size and color of scatters in (d)-(f) show corresponding observed $PM_{2.5}$ concentrations at 18 air quality monitoring stations.

Pollutant accumulation can regulate the PBL structure through the ARI, further exacerbating pollution (Wang et al., 2018; Miao et al., 2020). In the SCB, this positive feedback is weaker than in the other regions and may be inhibited by cloud radiation (Zhong et al., 2018). A series of simulation experiments were conducted to examine the aerosol radiation feedback in the SCB under the influence of two typical synoptic pollution patterns, as described in Section 2.4. BASE–EXP1 represents the perturbations caused by ARI, whereas EXP2–EXP3 demonstrates changes through ARI without CRI inhibition. Aerosols lead to surface cooling through absorbing and scattering solar radiation, thereby inhibiting the development of the PBL, which in turn facilitates pollutant accumulation (Fig. 12). Compared with Pattern 2, the aerosol concentrations in Pattern 5 were higher, resulting in greater reduction of downward solar radiation reduction due to ARI, leading to more pronounced cooling near the ground and a lower boundary layer height. Overall, the ARI in Pattern 5 was more significant than that in Pattern 2, regardless of CRI inhibition (Fig. 12).

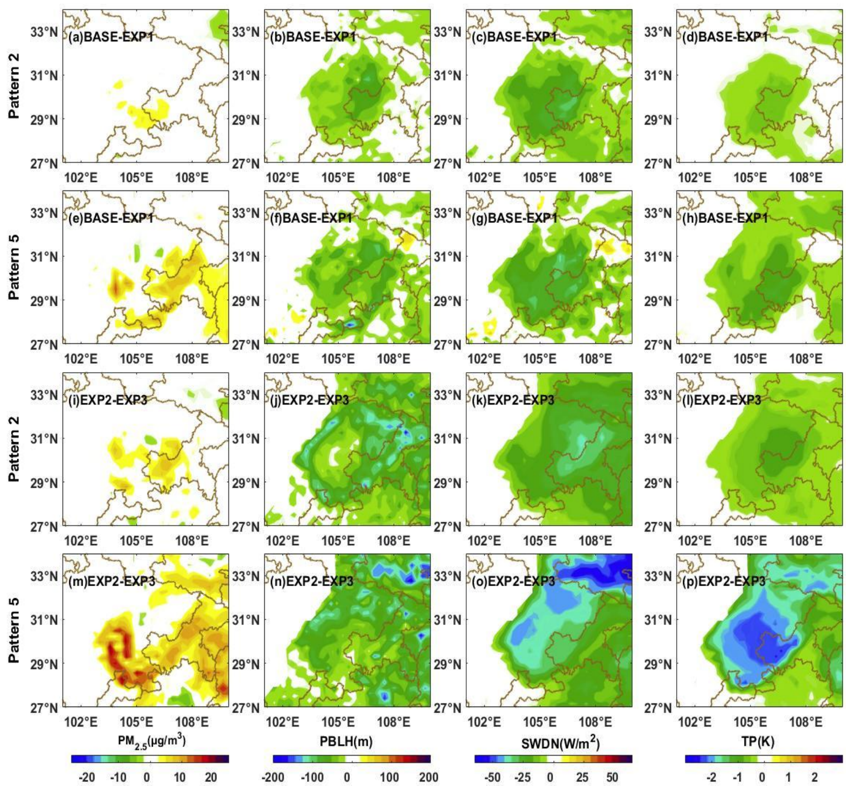

Figure 12. Spatial distribution of perturbations induced by (a)-(h) aerosol radiation interactions(ARI), and (i)-(p) ARI without the cloud radiation interaction(CRI) inhibition during 1-3 and 4-6 January representing Pattern 2 and Pattern 5 synoptic forcing, respectively.

https://doi.org/10.5194/egusphere-2023-1806
Preprint. Discussion started: 19 September 2023

Furthermore, results from parallel simulation experiments showed that the CRI significantly attenuated the ARI in the SCB under both pollution synoptic patterns. When the CRI is not considered, more solar radiation entered the PBL. Dense aerosols accumulating near the surface intercepted more downward shortwave radiation, resulting in stronger cooling near the ground and suppressing PBL development, contributing to a more remarkable ARI (Fig. 12). For the horizontal spatial distribution, a strong ARI was primarily observed in Chongqing, as well as the western and southern SCB, despite Chongqing experiencing lower pollutant concentrations than the other two regions (Figs. 8 and 11). This weaker ARI phenomenon in the western SCB was also reported by Zhong et al. (2019) and attributed to CRI inhibition of ARI. Considering the statistical results in Fig. 7, the average cloud liquid water contents in CD and YB were significantly higher than that in CQ under the influence of Patterns 2 and 5. Therefore, a more remarkable CRI inhibition would occur on the ARI in the western and southern SCB compared with CQ, leading to a relatively weaker ARI distribution in the region. Without considering the CRI, the ARI in the western and southern SCB would be much more pronounced than that in the CQ.

Using the western SCB, which exhibited the highest pollution concentration, as an example, Fig. 13 illustrates the vertical diurnal variations in temperature and solar radiation caused by the ARI. The results in Fig. 13 and 14 were derived from the simulation experiments in CD, as CD is one of the most polluted cities with typical meteorological and geographical characteristics of the western SCB. The ARI caused morning surface cooling and afternoon upper–air warming. As the local solar radiation increased from 8 am to 12 pm, the decrease in solar radiation caused by the ARI also increased, with surface cooling reaching its peak at approximately 10 am to 12 pm, gradually weakening in the afternoon. Wang et al. (2018) suggested that this was due to enhanced turbulence during morning PBL evolution. Afternoon surface cooling was partly compensated by the turbulent transport of warm air above the PBL. In addition, strong surface cooling between 5 pm and 8 pm in the SCB, is possibly influenced by remarkable valley wind circulations forced by the Qinghai–Tibet Plateau adjacent to the western SCB (Lu et al., 2022b). The evening cooling of the plateau induces strong mountain winds, promoting surface cooling, while the upper–layer warming mainly occurs around 1–1.5 km in the afternoon. In general, the ARI reduces solar radiation, causing surface cooling and upper air warming, thereby regulating the vertical atmospheric thermal structure, suppressing convection, and consequently decreasing PBL heights (Fig. 14).

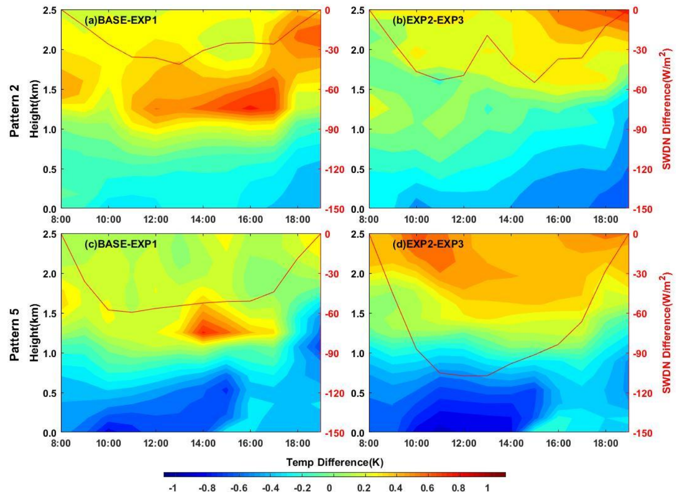

Figure 13. Diurnal variations of vertical temperature perturbations and downward solar radiation under influences of Pattern 2 and Pattern 5 induced by (a)(c)ARI and (b)(d)ARI without CRI inhibition.

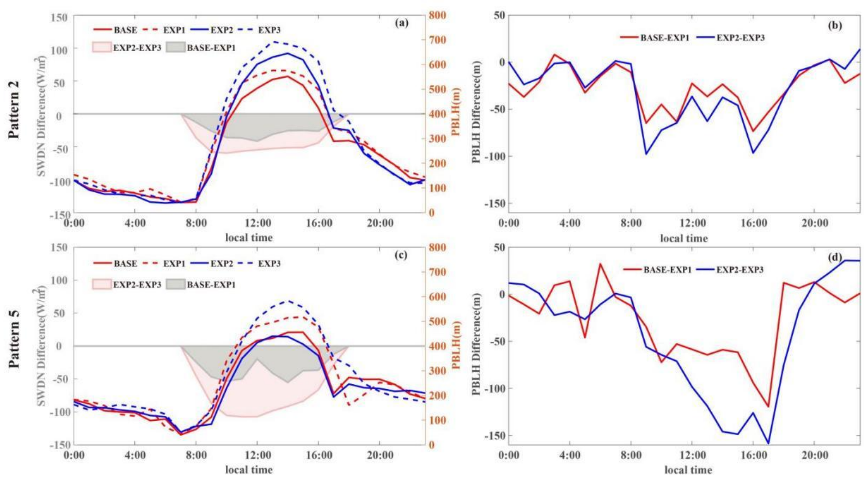

Figure 14. Diurnal variations of (a)(c)boundary layer height(lines) and downward solar radiation(shading), and (b)(d)the perturbations of boundary layer height induced by ARI and ARI without CRI inhibition, under Pattern 2 and Pattern 5 synoptic forcing respectively.

https://doi.org/10.5194/egusphere-2023-1806
Preprint. Discussion started: 19 September 2023

Synoptic patterns play a role in the interaction between the ARI and PBL (Wang et al., 2018; Miao et al., 2020). In the SCB, Pattern 5 suffered from denser aerosols due to the LT of Pattern 5 evolving from the low–pressure system in Pattern 2, and the accumulation of pollutants in Pattern 5 was based on Pattern 2 (Figs. 8 and 11). Denser aerosols under Pattern 5 caused a greater reduction in solar radiation, resulting in stronger surface cooling. During January 4–6, surface cooling reached 1 K, with cooling layers higher than those observed on January 1–3. The differences in thermal structure modulations contributed to a lower diurnal PBL height in Pattern 5 than in Pattern 2 (Figs. 14a and c), indicating that Pattern 5 was more favorable for ARI. Based on the simulation experiments, this study further discusses the impact of synoptic forcing on the CRI inhibition of ARI. When the CRI was not considered, the solar radiation reduction at noon on January 4–6 by the ARI was nearly twice as high as when the CRI was considered. Correspondingly, surface cooling at noon was remarkably enhanced. In the evening, surface cooling occurred earlier and was stronger without the CRI (Fig. 13). The regulation of CRI on ARI was further reflected in changes in PBL height. Without the CRI, the diurnal PBL height increased significantly, with the PBL height decreased more with ARI without CRI inhibition. The PBL heights were decreased by the ARI during January 13–17 afternoon, reaching 2–3 times the decrease observed with CRI inhibition (Fig. 14). More significant CRI inhibition of ARI was revealed under Pattern 5 compared with that under Pattern 2, owing to the stronger ARI itself with higher aerosol concentrations in Pattern 5 and the more apparent CRI inhibition with denser cloud liquid water contents under the LT pattern (Fig. 7). Therefore, the intensity of CRI inhibition of ARI in the SCB was altered by synoptic forcing, with stronger effects under the influence of LT.

https://doi.org/10.5194/egusphere-2023-1806
Preprint. Discussion started: 19 September 2023

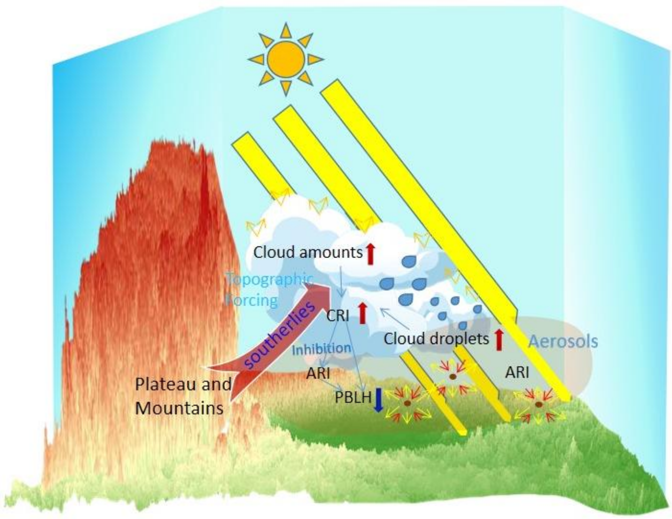

Figure 15. The Synergetic interactions of cloud, aerosol and radiation under the influence of cloudy pollution synoptic forcing.

4

4 Conclusion

This study conducted synoptic classification and numerical simulation to understand the combined effects of synoptic patterns and CRI inhibition on ARI and PBL structures in the wet and cloudy SCB. On the basis of long–term $PM_{2.5}$ observations and sounding data in the SCB, large-scale synoptic circulations on 850 hPa were indicated to play key roles in variations of $PM_{2.5}$ pollution. Synoptic classification was conducted with the T-PCA method, revealing that Pattern 2 and 5 characterized with low pressure system and southerly airflow on 850 hPa were key synoptic patterns for onset and accumulation of $PM_{2.5}$, while Pattern 1 controlled by the northerly airflow represented a clean pattern associated with significant decrease in $PM_{2.5}$. Moreover, denser cloud liquid water content and resulting stronger CRI could be found under Pattern 2 and 5. The highest cloud liquid water content and CRI appeared in Pattern 5, due to the robust southerly airflow induced by the dense isobaric lines, bringing warm and humid air masses and facilitating the conversion of aerosols to cloud/fog droplets.

To illustrate the interactions among cloud, aerosol and PBL under the pollution synoptic patterns, a pollution episode on January 1-7 of 2017 was simulated with using WRF-Chem. The

https://doi.org/10.5194/egusphere-2023-1806
Preprint. Discussion started: 19 September 2023

results showed that solar radiation was remarkably reduced by the ARI during the two pollution patterns, leading to morning surface cooling and afternoon upper–air warming. The enhanced evening surface cooling was impacted by the mountain–valley wind circulations forced by the plateau–basin topography of the SCB. This modulation in the vertical thermal structure by the ARI would then suppress the development of the PBL and favor pollution outbreaks (Fig. 15). Besides, the parallel simulation experiments also indicated that CRI impacted stratification stability and modulated the vertical thermal structure through its inhibition of the ARI (Fig. 15). For the spatial distribution, a stronger ARI appeared in Chongqing, despite lower $PM_{2.5}$ concentrations than in the western and southern SCB, because of the lower cloud liquid water content and weaker CRI inhibition of ARI in Chongqing. Without considering CRI inhibition, the ARI in the western and southern SCB was significantly stronger than that in Chongqing. In addition, the reduction in solar radiation and PBL height during daytime due to ARI could be more than doubled when neglecting the CRI influence under Pattern 5, primarily due to the higher aerosol concentrations and cloud liquid water contents with a low trough. This study revealed the interaction of multi–scale atmospheric physical processes in the SCB, considering its complex terrain and foggy/cloudy climate. The findings shed light on the interactions among aerosols, clouds, and PBL under different synoptic patterns and emphasize the significant role of CRI inhibition on ARI during wet and cloudy conditions.

Author contributions. HL and MX had the original idea for the study, designed the experiments, conducted the numerical simulation and prepared the initial draft manuscript. BL, YZ and KZ collected the data. TW and BZ helped perform the analysis with constructive discussions, reviewed and edited the manuscript. HL, MX, TW and BL acquired financial support for the project leading to this publication. SL and ML reviewed the manuscript.

Competing Interest: The authors declare no conflict of interest.

Data Available Statement

The ERA5 pressure layer and single layer data can be respectively downloaded from https://cds.climate.copernicus.eu/cdsapp#!/dataset/reanalysis-era5-pressure-levels and https://cds.climate.copernicus.eu/cdsapp#!/dataset/reanalysis-era5-single-levels?tab=form. The NCEP FNL data are available at https://rda.ucar.edu/datasets/ds083.2/. The MEIC data can be

https://doi.org/10.5194/egusphere-2023-1806
Preprint. Discussion started: 19 September 2023

accessed in Zheng et al(2018) at https://doi.org/10.5194/acp-18-14095-2018. Air quality and meteorological monitoring data can be acquired from https://doi.org/10.7910/DVN/USX59F.

Financial support: This work was supported by the National Natural Science Foundation of China (42205186), the Chongqing Natural Science Foundation (cstc2021jcyj-msxmX1007), the open research fund of Chongqing Meteorological Bureau (KFJJ-201607) and the key technology research and development of Chongqing Meteorological Bureau (YWJSGG-202215; YWJSGG-202303).

References

Alexeeff, S., Deosaransingh, K., Liao, N., Van Den Eeden, S., Schwartz, J., and Sidney, S. (2021) Particulate Matter and Cardiovascular Risk in Adults with Chronic Obstructive Pulmonary Disease, American journal of respiratory and critical care medicine 204(2): 159-167.

Cao, S., Zhang, S., Gao, C., Yan, Y., Bao, J., Su, L., Liu, M., Peng, N., and Liu, M. (2021) A long-term analysis of atmospheric black carbon MERRA-2 concentration over China during 1980–2019, Atmospheric Environment 264, 118662.

Chen, Z., Chen, D., Zhao, C., Kwan, M.-p., Cai, J., Zhuang, Y., Zhao, B., Wang, X., Chen, B., Yang, J., Li, R., He, B., Gao, B., Wang, K., and Xu, B. (2020) Influence of meteorological conditions on $PM_{2.5}$ concentrations across China: A review of methodology and mechanism, Environment International 139, 105558.

Ding, A., Huang, X., Nie, W., Sun, J., Kerminen, V.-M., Petäjä, T., Su, H., Cheng, Y., Yang, X.-Q., Wang, M., Chi, X., Wang, J. P., Virkkula, A., Guo, W., Yuan, J., Wang, S., Zhang, R. J., Wu, Y., Song, Y., and Fu, C. (2016) Black carbon enhances haze pollution in megacities in China, Geophysical Research Letters 43(6):2873-2879.

Garratt, J. R. (1994) Review: the atmospheric boundary layer, Earth-Science Reviews 37, 89-134.

Gong S, Liu Y, He J, Zhang L, Lu S, Zhang X. (2022)Multi-scale analysis of the impacts of meteorology and emissions on $PM_{2.5}$ and O_3 trends at various regions in China from 2013 to 2020 1: Synoptic circulation patterns and pollution. Sci Total Environ. Apr 1;815:152770.

Grell, G. A., Peckham, S. E., Schmitz, R., McKeen, S. A., Frost, G., Skamarock, W. C., and Eder, B. (2005) Fully coupled "online" chemistry within the WRF model, Atmospheric Environment 39, 6957-6975.

Grell, G. A., & Freitas, S. R. (2013). A scale and aerosol aware convective parameterization. Atmos. Chem. Phys, 14(10), 5233–5250.

https://doi.org/10.5194/egusphere-2023-1806
Preprint. Discussion started: 19 September 2023

Guenther, A., Karl, T., Harley, P., Wiedinmyer, C., Palmer, P. I., and Geron, C. (2006) Estimates of global terrestrial isoprene emissions using MEGAN (Model of Emissions of Gases and Aerosols from Nature), Atmos. Chem. Phys. 6, 3181-3210.

Guo, J., Miao, Y., Zhang, Y., Liu, H., Li, Z., Zhang, W., ... & Zhai, P. (2016) The climatology of planetary boundary layer height in China derived from radiosonde and reanalysis data. Atmospheric Chemistry and Physics, 16(20), 13309-13319.

Hansen, J., Sato, M., and Ruedy, R. (1997) Radiative forcing and climate response, 102, 6831-6864.

Haywood, J. M., Abel, S. J., Barrett, P. A., Bellouin, N., Blyth, A., Bower, K. N., Brooks, M., Carslaw, K., Che, H., Coe, H., Cotterell, M. I., Crawford, I., Cui, Z., Davies, N., Dingley, B., Field, P., Formenti, P., Gordon, H., de Graaf, M., Herbert, R., Johnson, B., Jones, A. C., Langridge, J. M., Malavelle, F., Partridge, D. G., Peers, F., Redemann, J., Stier, P., Szpek, K., Taylor, J. W., Watson-Parris, D., Wood, R., Wu, H., and Zuidema, P. (2021) The CLoud–Aerosol–Radiation Interaction and Forcing: Year 2017 (CLARIFY-2017) measurement campaign, Atmos. Chem. Phys. 21, 1049-1084.

Hong, S.-Y., Dudhia, J., and Chen, S.-H. (2004) A Revised Approach to Ice Microphysical Processes for the Bulk Parameterization of Clouds and Precipitation, Monthly Weather Review 132, 103-120.

Hong, S. Y., Y. Noh, and J. Dudhia (2006), A new vertical diffusion package with an explicit treatment of entrainment processes, Mon. Weather Rev., 134(9), 2318-2341.

Huth, R. (1996) AN INTERCOMPARISON OF COMPUTER-ASSISTED CIRCULATION CLASSIFICATION METHODS, International Journal of Climatology 16, 893-922.

Huth, R., Beck, C., Philipp, A., Demuzere, M., Ustrnul, Z., Cahynová, M., Kyselý, J., and Tveito, O. E. (2008) Classifications of Atmospheric Circulation Patterns, Ann N Y Acad Sci, 1146, 105-152.

Iacono, M. J., Delamere, J. S., Mlawer, E. J., Shephard, M. W., Clough, S. A., and Collins, W. D. (2008), Radiative forcing by long-lived greenhouse gases: Calculations with the AER radiative transfer models, J. Geophys. Res., 113, D13103.

Li, K., Liao, H., Mao, Y., and Ridley, D. A. (2016) Source sector and region contributions to concentration and direct radiative forcing of black carbon in China, Atmospheric Environment 124, 351-366.

Li, J., Wu, M., Li, Y., Ma, S., Wang, Z., Zhao, Y., et al. (2021a). Reinforcement of secondary circulation by aerosol feedback and $PM_{2.5}$ vertical exchange in the atmospheric boundary layer. Geophysical Research Letters, 48, e2021GL094465.

https://doi.org/10.5194/egusphere-2023-1806
Preprint. Discussion started: 19 September 2023

Li, Q., Wu, B., Liu, J., Zhang, H., Cai, X., and Song, Y. (2020) Characteristics of the atmospheric boundary layer and its relation with $PM_{2.5}$ during haze episodes in winter in the North China Plain, Atmospheric Environment 223, 117265.

Li, X., Miao, Y., Ma, Y., Wang, Y., and Zhang, Y. (2021b) Impacts of synoptic forcing and topography on aerosol pollution during winter in Shenyang, Northeast China, Atmospheric Research 262, 105764.

Li, Z., Wang, Y., Guo, J., Cribb, M., Dong, X., Fan, J., Gong, D.-Y., Huang, J., Jiang, M., Jiang, Y., Lee, S. S., Li, H., Li, J., Liu, J., Qian, Y., Rosenfeld, D., Shan, S., Sun, Y., Wang, H., and Zheng, Y. (2019) East Asian Study of Tropospheric Aerosols and their Impact on Regional Clouds, Precipitation, and Climate (EAST-AIR CPC), Journal of Geophysical Research: Atmospheres 124(23):13026-13054.

Liao, Z., Jielan, X., Fang, X., Wang, Y., Zhang, Y., Xu, X., and Fan, S. (2020) Modulation of synoptic circulation to dry season $PM_{2.5}$ pollution over the Pearl River Delta region: An investigation based on self-organizing maps, Atmospheric Environment 230, 117482.

Liu, N., Zhou, S., Liu, C., and Guo, J. (2019) Synoptic circulation pattern and boundary layer structure associated with $PM_{2.5}$ during wintertime haze pollution episodes in Shanghai, Atmospheric Research 228, 186-195.

Lohmann, U., and Feichter, J. (2005) Global indirect aerosol effects: a review, Atmos. Chem. Phys. 5, 715-737.

Lu H, Xie M, Liu B, Liu X, Feng J, Yang F, Zhao X, You T, Wu Z, Gao Y. (2022a) Impact of atmospheric thermodynamic structures and aerosol radiation feedback on winter regional persistent heavy particulate pollution in the Sichuan-Chongqing region, China. Sci Total Environ. Oct 10;842:156575.

Lu, H., Xie, M., Liu, X., Liu, B., Liu, C., Zhao, X., Du, Q., Wu, Z., Gao, Y., and Xu, L. (2022b) Spatial-temporal characteristics of particulate matters and different formation mechanisms of four typical haze cases in a mountain city, Atmospheric Environment, 269, 118868.

Ma, S., Shao, M., Zhang, Y., Dai, Q., and Xie, M. (2021) Sensitivity of $PM_{2.5}$ and O_3 pollution episodes to meteorological factors over the North China Plain, Science of The Total Environment 792, 148474.

Miao, Y., Che, H., Zhang, X., and Liu, S. (2020) Integrated impacts of synoptic forcing and aerosol radiative effect on boundary layer and pollution in the Beijing–Tianjin–Hebei region, China, Atmos. Chem. Phys. 20, 5899-5909.

Miao, Y., Che, H., Zhang, X., and Liu, S. (2021) Relationship between summertime concurring $PM_{2.5}$ and O_3 pollution and boundary layer height differs between Beijing and Shanghai, China, Environmental Pollution 268, 115775.

https://doi.org/10.5194/egusphere-2023-1806
Preprint. Discussion started: 19 September 2023

Miao, Y., Guo, J., Liu, S., Liu, H., Li, Z., Zhang, W., and Zhai, P. (2017) Classification of summertime synoptic patterns in Beijing and their associations with boundary layer structure affecting aerosol pollution, Atmospheric Chemistry and Physics 17, 3097-3110.

Ning, G., Wang, S., Ma, M., Ni, C., Shang, Z., Wang, J., and Li, J. (2017) Characteristics of air pollution in different zones of Sichuan Basin, China, The Science of the total environment 612, 975-984.

Ning, G., Yim, S. H. L., Wang, S., Duan, B., Nie, C., Yang, X., Wang, J., and Shang, K. (2019) Synergistic effects of synoptic weather patterns and topography on air quality: a case of the Sichuan Basin of China, Climate Dynamics 53, 6729-6744.

Pilinis, C., Seinfeld, J. H., and Grosjean, D. (1989) Water content of atmospheric aerosols, Atmospheric Environment 23, 1601-1606.

Pöschl, U., Martin, S. T., Sinha, B., Chen, Q., Gunthe, S. S., Huffman, J. A., Borrmann, S., Farmer, D. K., Garland, R. M., Helas, G., Jimenez, J. L., King, S. M., Manzi, A., Mikhailov, E., Pauliquevis, T., Petters, M. D., Prenni, A. J., Roldin, P., Rose, D., Schneider, J., Su, H., Zorn, S. R., Artaxo, P., and Andreae, M. O. (2010) Rainforest Aerosols as Biogenic Nuclei of Clouds and Precipitation in the Amazon, 329, 1513-1516.

Rosenfeld, D., Lohmann, U., Raga, G. B., O'Dowd, C. D., Kulmala, M., Fuzzi, S., Reissell, A., and Andreae, M. O. (2008) Flood or Drought: How Do Aerosols Affect Precipitation?, Science 321, 1309-1313.

Schell, B., Ackermann, I. J., Hass, H., Binkowski, F. S., and Ebel, A. (2001) Modeling the formation of secondary organic aerosol within a comprehensive air quality model system, Journal of Geophysical Research: Atmospheres 106, 28275-28293.

Scott Archer-Nicholls, Douglas Lowe, David M. Schultz, and Gordon McFiggans. (2016)Aerosol–radiation–cloud interactions in a regional coupled model: the effects of convective parameterisation and resolution, Atmos. Chem. Phys., 16, 5573–5594.

Shu, Z., Liu, Y., Zhao, T., Xia, J., Wang, C., Cao, L., Wang, H., Zhang, L., Zheng, Y., Shen, L., Luo, L., and Li, Y. (2021) Elevated 3D structures of $PM_{2.5}$ and impact of complex terrain-forcing circulations on heavy haze pollution over Sichuan Basin, China, Atmos. Chem. Phys. 21, 9253-9268.

Stockwell, W. R., Middleton, P., Chang, J. S., and Tang, X. (1990) The second generation regional acid deposition model chemical mechanism for regional air quality modeling, Journal of Geophysical Research: Atmospheres 95, 16343-16367.

https://doi.org/10.5194/egusphere-2023-1806
Preprint. Discussion started: 19 September 2023

Su, T., Li, Z., and Kahn, R. (2018) Relationships between the planetary boundary layer height and surface pollutants derived from lidar observations over China: regional pattern and influencing factors, Atmos. Chem. Phys. 18, 15921-15935.

Tewari, M., Chen, F., Wang, W., Dudhia, J., Lemone, M. A., … Mitchell, K. E. (2004). Implementation and verification of the unified Noah land-surface model in the WRF model [presentation]. In 20th Conference on Weather Analysis and Forecasting/16th Conference on Numerical Weather Prediction. American Meteorological Society: Seattle, WA, US.

Twomey, S. (1977) The Influence of Pollution on the Shortwave Albedo of Clouds, Journal of Atmospheric Sciences 34, 1149-1152.

Wang, C., Jia, M., Xia, H., Wu, Y., Wei, T., Shang, X., Yang, C., Xue, X., and Dou, X. (2019) Relationship analysis of $PM_{2.5}$ and boundary layer height using an aerosol and turbulence detection lidar, Atmos. Meas. Tech. 12, 3303-3315.

Wang, Z., Huang, X., and Ding, A. (2018) Dome effect of black carbon and its key influencing factors: a one-dimensional modelling study, Atmos. Chem. Phys. 18, 2821-2834.

Wang, Y., Gao, W., Wang, S., Song, T., Gong, Z., Ji, D., Wang, L., Liu, Z., Tang, G., Huo, Y., Tian, S., Li, J., Li, M., Yang, Y., Chu, B., Petäjä, T., Kerminen, V.-M., He, H., Hao, J., Kulmala, M., Wang, Y., and Zhang, Y. (2020) Contrasting trends of $PM_{2.5}$ and surface-ozone concentrations in China from 2013 to 2017, National Science Review 7, 1331-1339.

Xiao, Q., Zheng, Y., Geng, G., Chen, C., Huang, X., Che, H., Zhang, X., He, K., and Zhang, Q. (2021) Separating emission and meteorological contributions to long-term $PM_{2.5}$ trends over eastern China during 2000–2018, Atmos. Chem. Phys. 21, 9475-9496.

Xie, M., Liao, J., Wang, T., Zhu, K., Zhuang, B., Han, Y., Li, M., and Li, S. (2016) Modeling of the anthropogenic heat flux and its effect on regional meteorology and air quality over the Yangtze River Delta region, China, Atmospheric Chemistry and Physics 16, 6071-6089.

Xie, M., Zhu, K., Wang, T., Feng, W., Gao, D., Li, M., Li, S., Zhuang, B., Han, Y., Chen, P., and Liao, J. (2016) Changes in regional meteorology induced by anthropogenic heat and their impacts on air quality in South China, Atmos. Chem. Phys. 16, 15011-15031.

Xu, Y., Xue, W., Lei, Y., Huang, Q., Zhao, Y., Cheng, S., Ren, Z., and Wang, J. (2020) Spatiotemporal variation in the impact of meteorological conditions on $PM_{2.5}$ pollution in China from 2000 to 2017, Atmospheric Environment 223, 117215.

Yang, T., Chen, R., Gu, X., Xu, J., Yang, L., Zhao, J., Zhang, X., Bai, C., Kang, J., Ran, P., Shen, H., Wen, F., Huang, K., Chen, Y., Sun, T., Shan, G., Lin, Y., Wu, S., Zhu, J., Wang, R., Shi, Z., Xu, Y., Ye, X., Song, Y., Wang, Q., Zhou, Y., Ding, L., Yang, T., Yao, W., Guo, Y., Xiao, F., Lu, Y., Peng, X., Zhang, B., Xiao, D., Wang, Z., Zhang, H., Bu, X., Zhang, X., An, L., Zhang, S., Cao, Z., Zhan, Q., Yang, Y., Liang, L., Cao, B., Dai, H., van Donkelaar, A., Martin, R. V., Wu, T., He, J., Kan, H., and Wang, C. (2021) Association of fine particulate matter air pollution and its constituents with lung function: The China Pulmonary Health study, Environment International 156, 106707.

Yang Dasheng, Wang Pucai. 2012. Characteristics of Vertical Distributions of Cloud Water Contents over China during Summer. Chinese Journal of Atmospheric Sciences, 36(1): 89-101.

Yin, Z., and Wang, H. (2017) Role of atmospheric circulations in haze pollution in December 2016, Atmos. Chem. Phys. 17, 11673-11681.

Yu, R., Wang, B., and Zhou, T. (2004) Climate Effects of the Deep Continental Stratus Clouds Generated by the Tibetan Plateau, Journal of Climate 17, 2702-2713.

Zhan, C.-c., Xie, M., Fang, D.-x., Wang, T., Wu, Z., Lu, H., Li, M.-m., Chen, P., Zhuang, B.-l., Li, S., Zhang, Z.-q., Gao, D., Reng, J.-y., and Zhao, M. (2019) Synoptic weather patterns and their impacts on regional particle pollution in the city cluster of the Sichuan Basin, China, Atmospheric Environment 208(1): 34-47.

Zhan, C., Xie, M., Lu, H., Liu, B., Wu, Z., Wang, T., Zhuang, B., Li, M., and Li, S.(2023) Impacts of urbanization on air quality and the related health risks in a city with complex terrain, Atmos. Chem. Phys., 23, 771–788,

Zhang, J., Lin, Z., 1985. Climate in China. Shanghai Publication House, Shanghai, p. 603.

Zhang, S., Zeng, G., Wang, T., Yang, X., and Iyakaremye, V. (2022) Three dominant synoptic atmospheric circulation patterns influencing severe winter haze in eastern China, Atmos. Chem. Phys. 22, 16017-16030.

Zhang, Y., Ding, A., Mao, H., Nie, W., Zhou, D., Liu, L., Huang, X., and Fu, C. (2015) Impact of synoptic weather patterns and inter-decadal climate variability on air quality in the North China Plain during 1980–2013, Atmospheric Environment 124, Part B: 119-128.

Zhao, B., Liou, K.-N., Gu, Y., Li, Q., Jiang, J. H., Su, H., He, C., Tseng, H.-L. R., Wang, S., Liu, R., Qi, L., Lee, W.-L., and Hao, J. (2017) Enhanced $PM_{2.5}$ pollution in China due to aerosol-cloud interactions, Scientific Reports 7, 4453.

https://doi.org/10.5194/egusphere-2023-1806
Preprint. Discussion started: 19 September 2023

Zhao, C., Yang, Y., Fan, H., Huang, J., Fu, Y., Zhang, X., Kang, S., Cong, Z., Letu, H., and Menenti, M. (2020) Aerosol characteristics and impacts on weather and climate over the Tibetan Plateau, National Science Review 7, 492-495.

Zhao, S., Yu, Y., Yin, D., Qin, D., He, J., and Dong, L. (2017) Spatial patterns and temporal variations of six criteria air pollutants during 2015 to 2017 in the city clusters of Sichuan Basin, China, The Science of the total environment 624, 540-557.

Zheng, B., Tong, D., Li, M., et al. (2018) Trends in China's anthropogenic emissions since 2010 as the consequence of clean air actions, Atmos. Chem. Phys., 18, 14095-14111.

Zhong, J., Zhang, X., Wang, Y., Wang, J., Shen, X., Zhang, H., Wang, T., Xie, Z., Liu, C., Zhang, H., Zhao, T., Sun, J., Fan, S., Gao, Z., Li, Y., and Wang, L. (2019) The two-way feedback mechanism between unfavorable meteorological conditions and cumulative aerosol pollution in various haze regions of China, Atmospheric Chemistry and Physics 19, 3287-3306.

Zhong, J., Zhang, X., Yunsheng, D., Wang, Y., Liu, C., Wang, J., Zhang, Y., and Che, H. (2018) Feedback effects of boundary-layer meteorological factors on cumulative explosive growth of $PM_{2.5}$ during winter heavy pollution episodes in Beijing from 2013 to 2016, Atmospheric Chemistry and Physics 18, 247-258.

Zhou, M., Zhang, L., Chen, D., Gu, Y., Fu, T.-M., Gao, M., Zhao, Y., Lu, X., and Zhao, B. (2019) The impact of aerosol–radiation interactions on the effectiveness of emission control measures, Environmental Research Letters 14, 024002.